Appendix H
NONLINEAR TIME HISTORY ANALYSIS OF GRAVITY DAMS

H-1. Introduction

The example problem is a 74 m (243.33 ft) high non-overflow gravity dam section with a crest thickness of 9.75 m (32 ft) and a base thickness of 53.83 m (176.6 ft). On the lower two-third, the dam is sloped at 1/10 on the upstream and at 7/10 on the downstream face. The dam is first analyzed using linear time-history method to illustrate the linear-elastic acceptance criteria discussed in Paragraph 6.4*d*(1), and then evaluated by nonlinear time-history method to assess potential sliding and rocking responses under earthquake shaking.

H-2. Purpose and Objectives

The purpose of this example is to illustrate the application of linear and nonlinear time history methods to earthquake response analysis of gravity dams. The objectives of this study are: 1) to compute displacements and stresses for four sets of earthquake acceleration time histories, 2) to identify main nonlinear mechanisms and potential failure modes, 3) to perform nonlinear analysis with the identified nonlinear mechanisms, and 4) to assess stability condition of the dam.

H-3. Scope

The scope of this example includes the following:

a. Establishment of evaluation earthquake and associated acceleration time histories.

b. Computation of linear earthquake response of the dam including the effects of foundation and impounded water.

c. Evaluation of results of linear time history with the acceptance criteria.

d. Development of nonlinear model with the main nonlinear mechanisms.

e. Evaluation of nonlinear time-history analyses to assess stability of the dam.

H-4. Earthquake Ground Motions

For evaluation of the earthquake response using linear ad nonlinear time-history analyses, the example gravity dam was assumed to be located in the near field of a maximum earthquake event having a moment magnitude M_w of about 6-1/2. Four sets of recorded acceleration time-histories from three earthquakes were selected in accordance with procedures discussed in Chapter 5 of EM 1110-2-6051. These included the Pacoima Dam record from 1971 San Fernando earthquake, the Gilroy Array No. 1 record from 1989 Loma Prieta earthquake, the Newhall record from 1994 Northridge earthquake, and the 1971 Pacoima Dam record modified to match the design response spectra. The design response spectra for the horizontal and vertical components of ground motion are the same as those used in Example D3. The ground motions were scaled such that the sum of ordinates for the response spectra of each natural record would match the sum for the smooth response spectra in the period range of 0.06 to 0.3 sec. The response spectra for the scaled records are compared with the smooth design response spectra in Figure H-1. Time-histories of the horizontal components of the records are

plotted in Figure H-2. This figure clearly demonstrates the pulsive ("fling") type motions contained in the San Fernando and Northridge records.

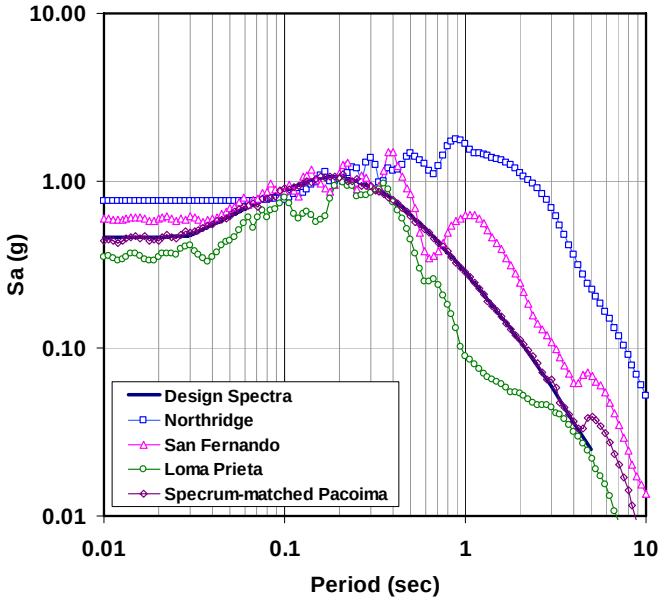

Figure H-1. Comparison of design response spectra with spectra of scaled records

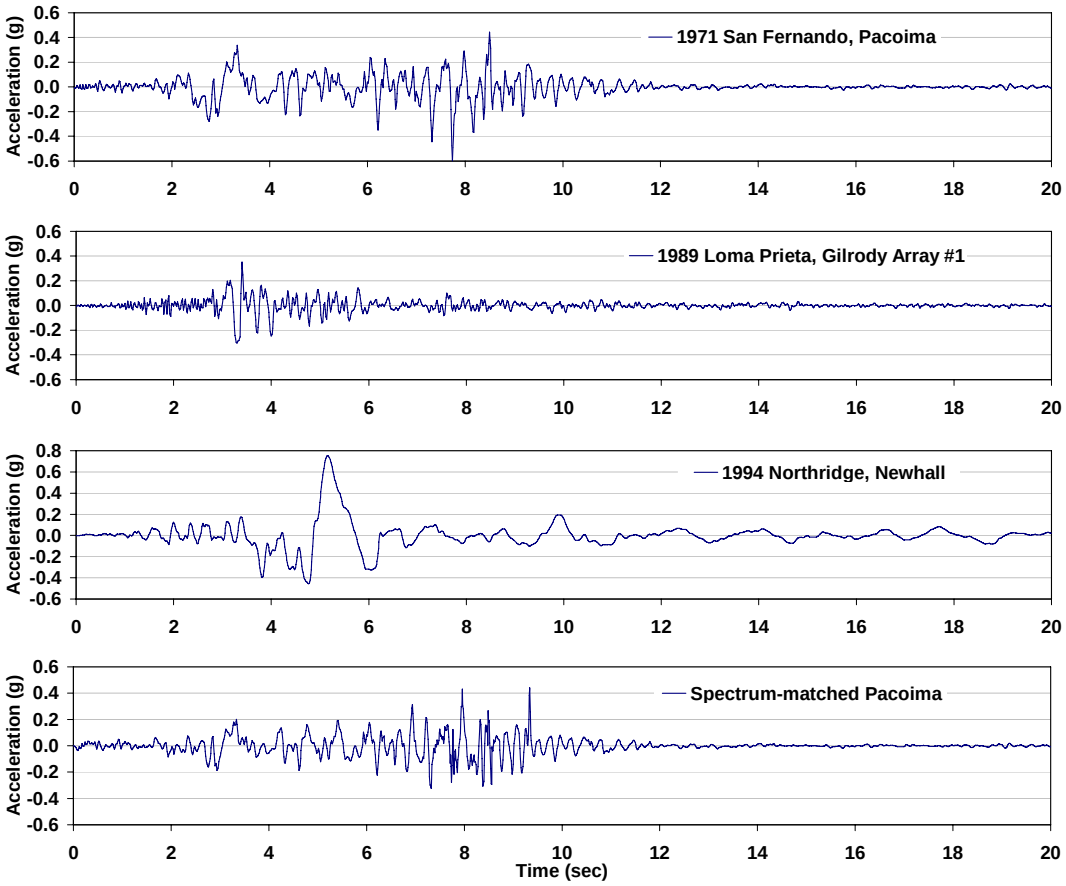

Figure H-2. Horizontal component of earthquake input acceleration time histories

H-5. Linear Elastic Response

a. Finite-element model. The linear-elastic time-history analysis of the example dam was carried out in accordance with Paragraphs 4.3*a*(3) and 6.3*d*(2). The dam and foundation rock were represented by 2D shell elements of unit thickness with concrete and rock properties, respectively. A modulus of elasticity of 282.5 MPa (5.9×10^6 psi), a Poisson's ratio of 0.19, with a unit weight of 2530.9 kg/m^3 (158 pcf) was assumed for the mass concrete. The foundation rock was assumed massless but its modulus and Poisson's ratio were assumed to be respectively 277.7 MPa (5.8×10^6 psi) and 0.19. The inertia forces of the impounded water were represented by added hydrodynamic mass values in accordance with the generalized Westergaard method (see EM 1110-2-6051). The added mass associated with nodal points on the sloped portion of the upstream face consists of horizontal and vertical values. Thus they generate inertia forces in the horizontal and vertical directions. The finite-element model is shown in Figure H-3. A total of 3,417 shell elements were used: 1,493 elements to model the dam, and 1,924 to model the foundation rock. The model included a total number of 3,612 nodal points.

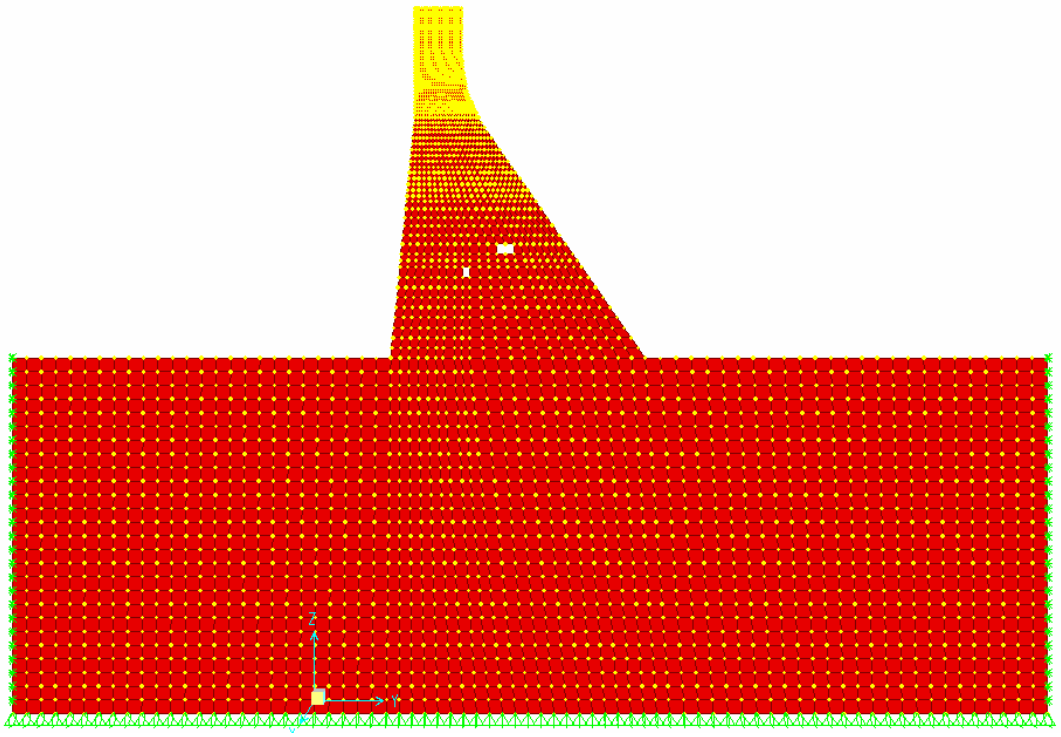

Figure H-3. SAP2000 dam-foundation model

b. Evaluation of Linear Response. The example dam model was analyzed for the combined effects of static plus seismic loads. The static loads included the gravity due to deadweight of the concrete, hydrostatic pressures corresponding to a headwater depth of 73.15 m (240 ft with water level at 3.33 feet below the crest of the dam), and uplift pressures. The earthquake loads consisted of the inertia forces generated by earthquake ground motions described in Paragraph H-4. A linear uplift pressure distribution from 240-ft headwater to zero tailwater was assumed. The uplift pressure was also assumed not to change during the earthquake ground shaking. The results of analyses include envelopes of maximum stresses, time history of stresses, time history of displacements, and time history of reaction forces at the dam-foundation contact. The envelopes of maximum stresses are used to assess severity and extent of overstressed regions. The stress time histories are used to compute cumulative duration of stress excursions for comparison with the acceptance limits. Finally, time histories of reaction forces are used to compute instantaneous factors of safety to assess stability conditions of the dam.

(1) *Envelopes of maximum stresses*. Figure H-4 displays envelopes of maximum vertical stresses for the four earthquake acceleration time histories. The results indicate that high tensile stresses generally develop at the heel and toe of the dam as well as at upper elevations near the change of slopes of the upstream and downstream faces. In terms of the magnitude and spatial extent, high tensile stresses are most severe for the 1971 San Fernando record, where they cover more than 80 percent of the upstream face of the dam. Recognizing that the tensile strength at the dam-rock contact is lower than the tensile strength of the concrete, the cracking is expected to initiate at the heel of the dam and propagate toward the toe. Tensile cracking at the base of the dam causes sliding, but at the same time reduces tensile stresses at locations above the base. This tentative nonlinear behavior will be substantiated by the nonlinear time-history analysis in Paragraph H-6.

(2) *Time history of maximum stresses*. Figure H-5a shows time history plots of maximum stresses at the heel (Element 4001) of the dam and at the downstream change of slope (Element 4767). Also shown on these plots are the static tensile strength of 2.9 MPa (425 psi) and apparent dynamic tensile strength of 5.8 MPa (850 psi) for the concrete. Note that for computation of cumulative duration, the 2.9 MPa (425 psi) corresponds to DCR = 1 and 5.8 MPa (850 psi) to DCR = 2. The results show that stresses at the heel of the dam exceed DCR = 1 and 2. The number of stress cycles exceeding DCR = 2 is 15. This suggests that cracking initiates and propagates from the heel of the dam. The stresses at the top of the dam, even though large, remain below DCR = 2 and may not cause cracking because their magnitudes will be reduce as soon as cracking develops at the base of the dam. This observation will be substantiated by the nonlinear analysis in Paragraph H-6 below.

(3) *Time history of maximum displacements*. Time histories of horizontal displacements at the top of the dam are provided in Figure H-5b for the four earthquake records. At 47.5 mm (1.87 in.), the largest displacement occurs for the San Fernando record, followed with 40.4 mm (1.59 in.) for the spectrum-matched Pacoima, 38.8 mm (1.53 in.) for Northridge, and 35 mm (1.38 in.) for the Loma Prieta records.

(4) *Comparison with acceptance criteria*. The acceptance criteria for the linear time-history evaluation of gravity dams are that the percentage of the overstressed regions and cumulative duration of stress cycles above the tensile strength of the concrete remain below the performance curves given in Paragraph 6.4d(1). As discussed above, the static tensile strength and the apparent dynamic tensile strength of the concrete represent the range of acceptable tensile stress magnitudes. Knowing the static tensile strength of the concrete the surface areas with tensile stresses above demand-capacity ratios of 1, 1.2, 1.4, 1.6, 1.8, and 2 were estimated from the stress contour plots. A plot of the results in Figure H-6 shows that the overstressed areas exceed the acceptance limit for three of the earthquake records; only overstressed areas for the Loma Prieta record fall below the acceptance curve. Figure H-7 compares cumulative duration of stress cycles for Element 4001 at the heel of the dam with the acceptance curve. It is obvious that all cumulative duration for this element exceed the acceptance limits. In addition to Element 4001, the cumulative duration was also computed for four other elements near the heel and toe of the dam, as identified in Figure H-8. The cumulative duration for these elements is compared with the acceptance limits in Figure H-9. The results show that only the cumulative duration for two elements near the heel and one element at the toe exceed the acceptance limits. This suggests that cracking initiates from the heel and toe of the dam but may or may not propagate through the entire base. Thus, a nonlinear time history analysis is needed to evaluate the crack propagation and the effects it may have on sliding of the dam, as discussed in Paragraph H-6.

(5) *Seismic stability condition*. The normal and horizontal forces along the dam-foundation contact were obtained to assess sliding stability condition of the dam. Time histories of vertical (normal) and horizontal (shear) forces were computed by the SAP2000 computer program for the combined effects of gravity, hydrostatic, uplift, and the earthquake loads. The resultant vertical and horizontal reaction forces are displayed in the upper and mid graphs of Figure H-10. Knowing the normal and shear forces and assuming a friction coefficient of unity, the instantaneous sliding factors of safety were computed in accordance with Paragraph 7-3c(1), as shown in bottom graph of Figure H-10. Note that the instantaneous factor of safety at the time of zero represents the static sliding factor of safety, which for this example is 1.2. During the earthquake ground shaking the instantaneous factor of safety oscillates above and below the value of the static factor of safety as the magnitude and direction of inertia force changes. Figure H-10 shows that the instantaneous factor of safety repeatedly falls below unity, an

indication that the dam will slide along its base. The magnitude of sliding displacement however, is estimated using the nonlinear time-history analysis described in Paragraph H-6.

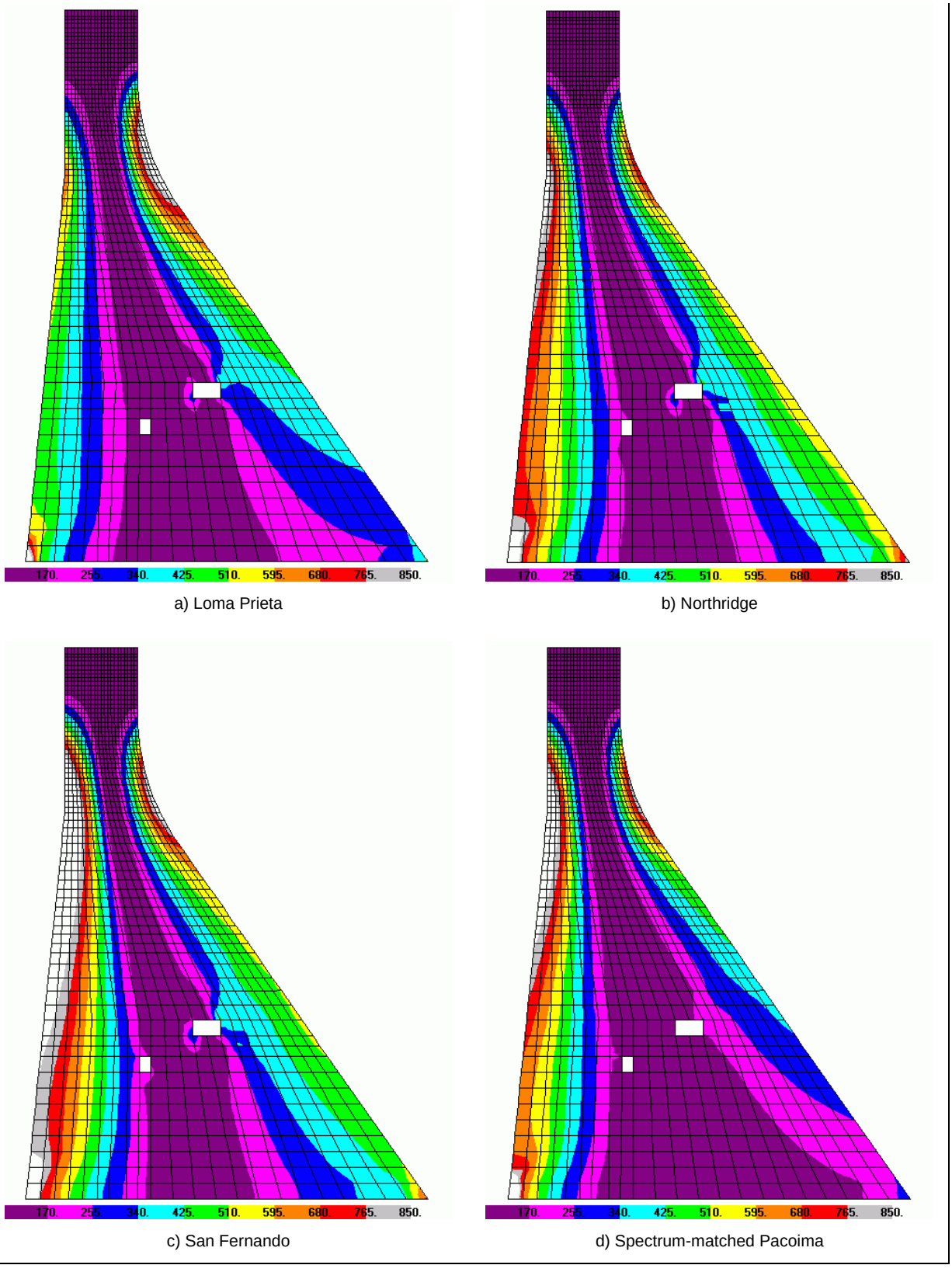

Figure H-4. Envelopes of maximum vertical stresses from linear TH analysis (psi)

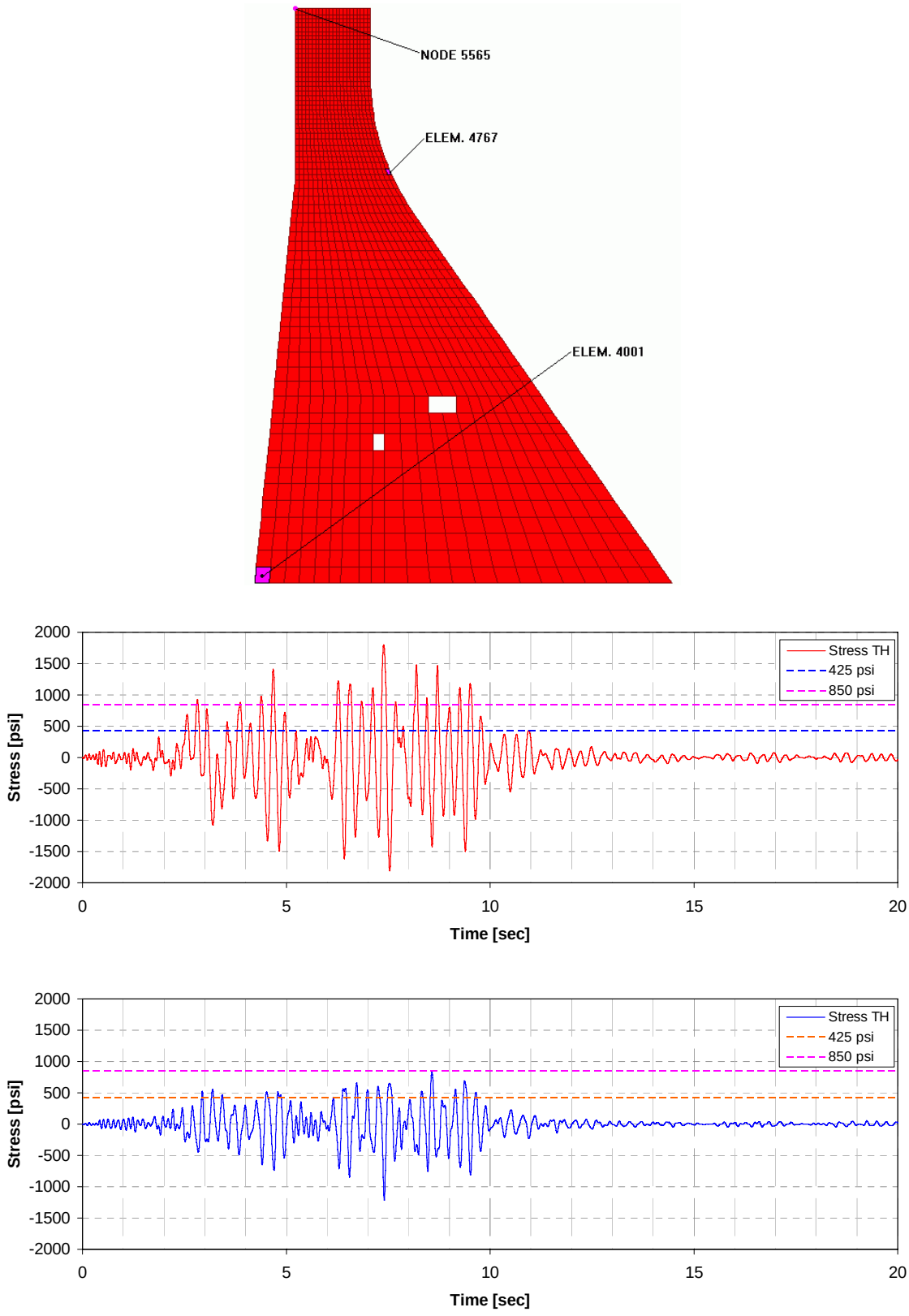

Figure H-5a. Time history of maximum vertical stresses at the heel of the dam (Elem. 4001) and at the change of slope on downstream face (Elem. 4767) for San Fernando seismic input

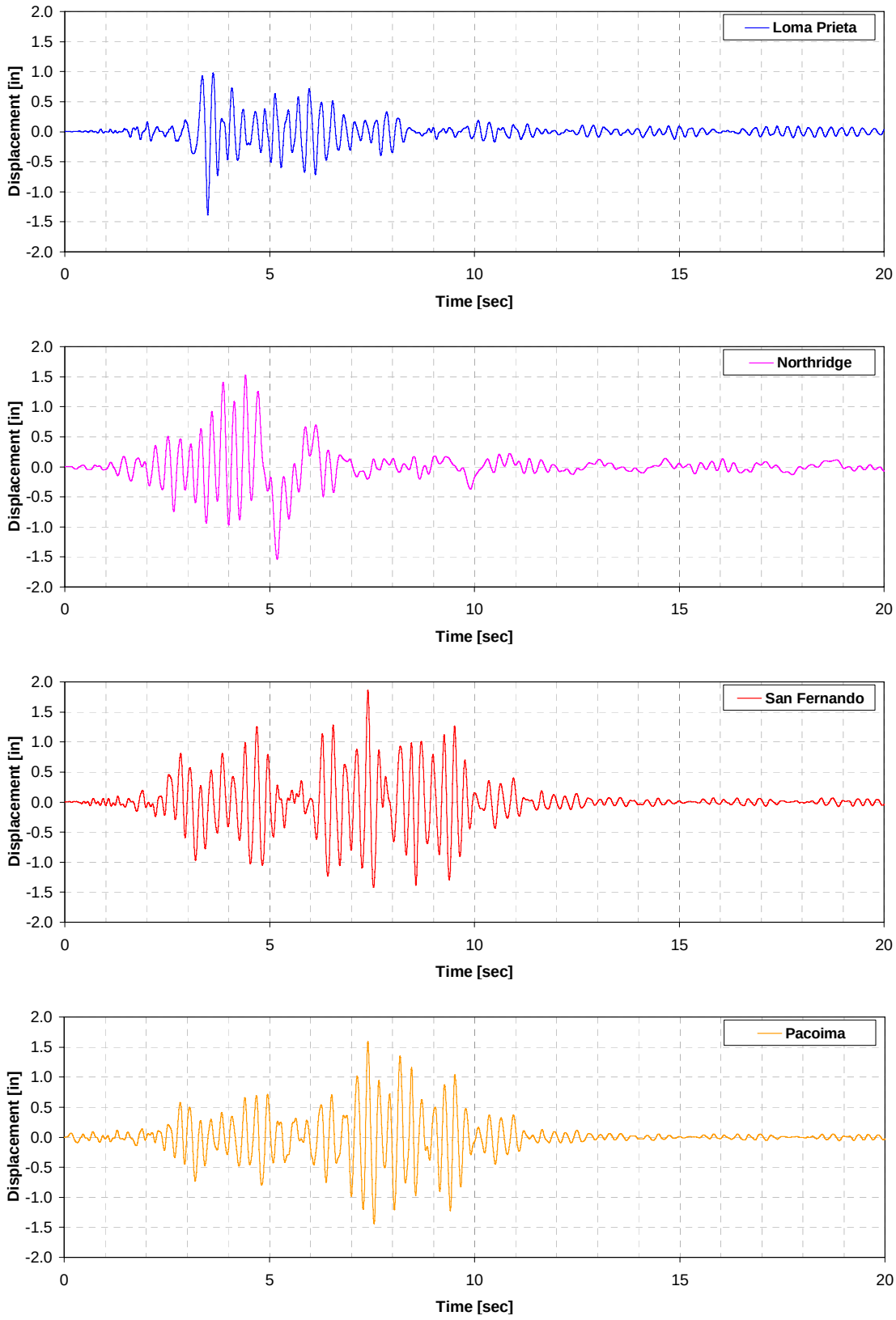

Figure H-5b. Time history of horizontal displacement at top of the dam (Node 5565 in Figure H-5a)

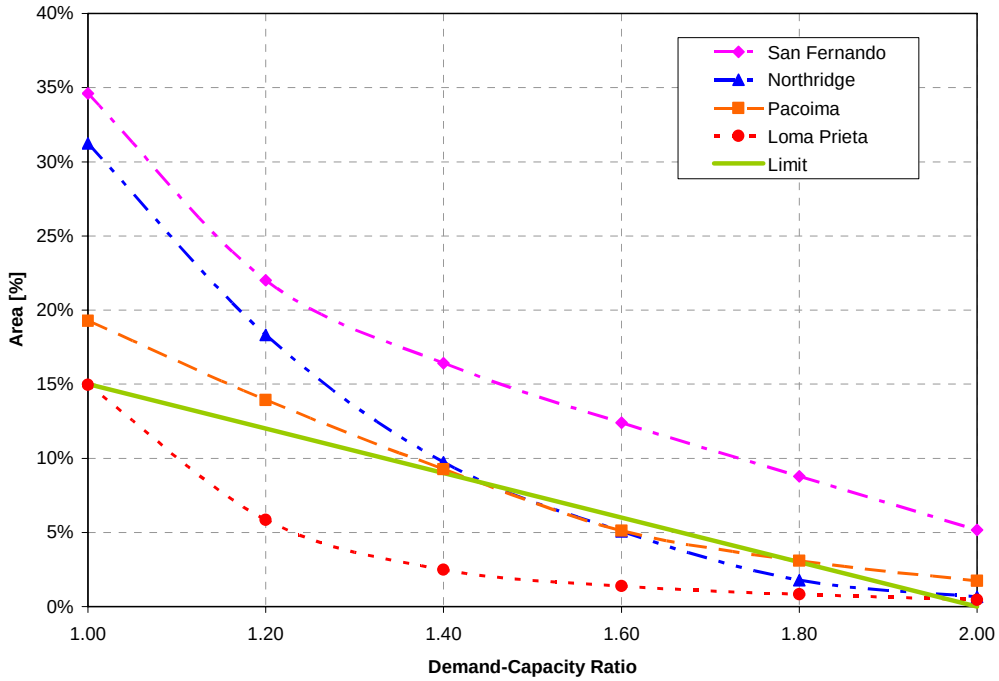

Figure H-6. Comparison of percentage of overstressed areas with acceptance limits

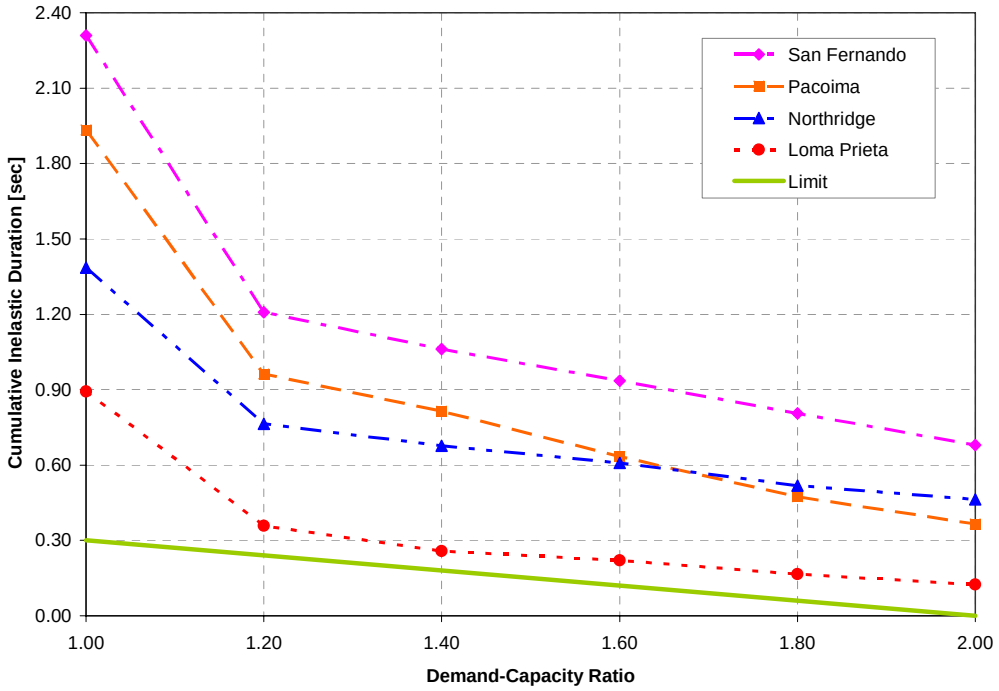

Figure H-7. Comparison of cumulative duration of stress cycles with acceptance limits for stresses at the heel of the dam (Element 4001 in Figure H-8)

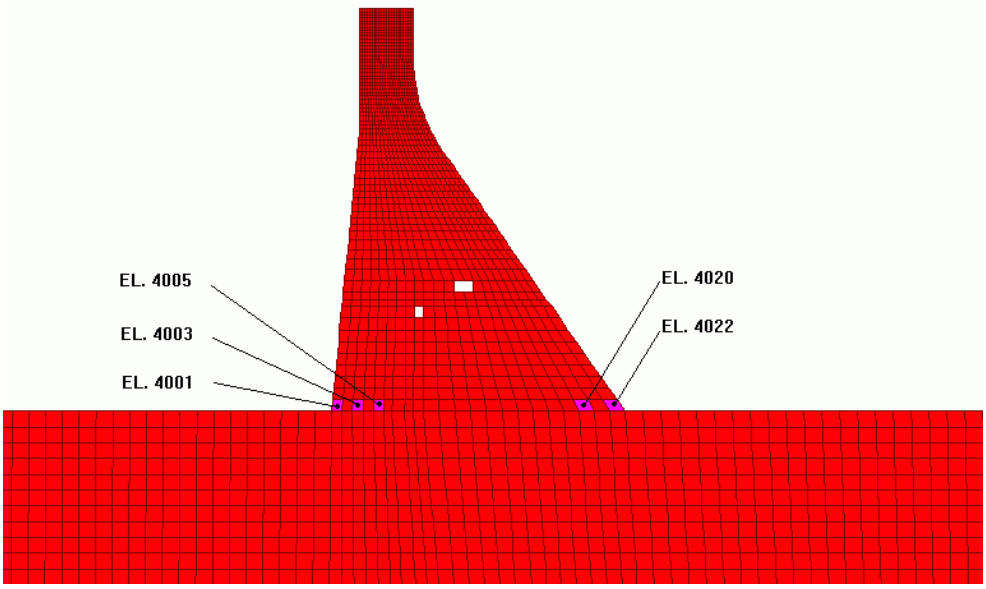

Figure H-8. Elements for which cumulative duration are shown in Figure H-9

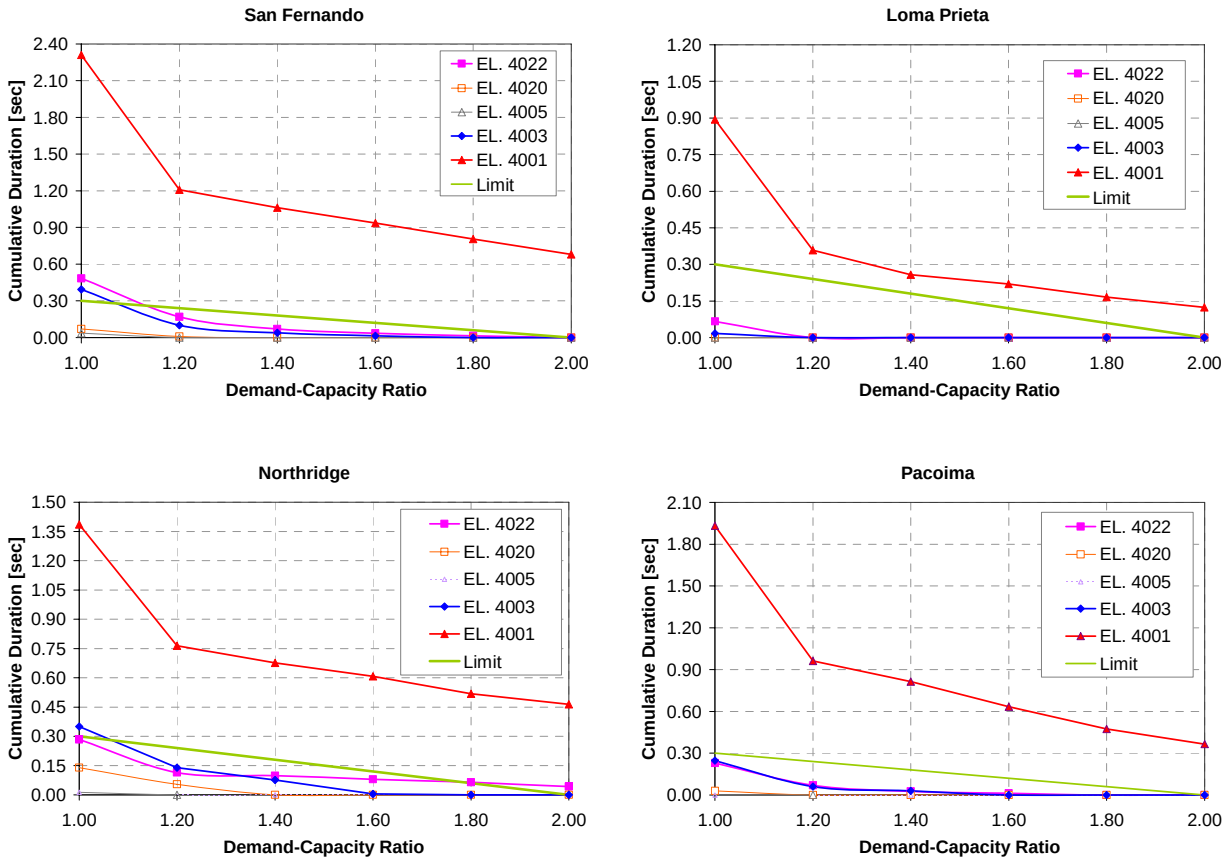

Figure H-9. Comparison of cumulative duration with performance curve for elements shown in Figure H-8

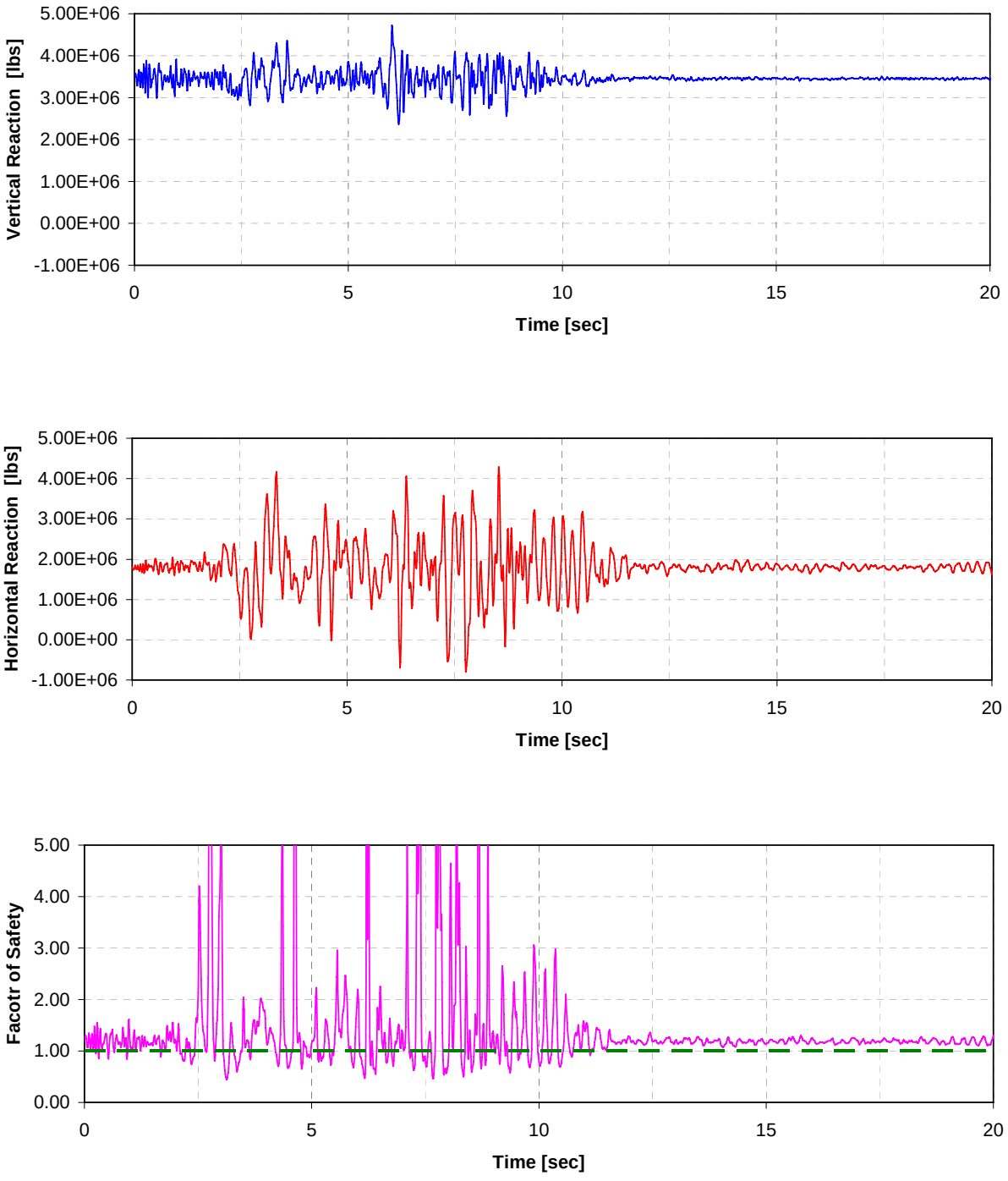

Figure H-10. Time histories of vertical (top graph) and horizontal (middle graph) resultant reaction forces used to compute instantaneous factors of safety (bottom graph). Results shown are for San Fernando record

H-6. Nonlinear Response Analysis

a. Selection of Nonlinear Analysis Procedure. The results of linear analysis indicate that high tensile stresses develop at the base of the dam, on the upstream face of the dam, and on the downstream face near the change of slope. The magnitudes of stresses are generally higher at the base of the dam than they are at the upper elevations. For this reason and also because tensile strength of the dam-rock contact is expected to be lower than that of the concrete, the nonlinear response in the form of tensile cracking is likely to start at the base. The nonlinear analysis of the dam should therefore be formulated to capture this nonlinear mechanism. In this example, gap-friction elements are introduced at the base of the dam to simulate cracking and the sliding and rocking responses that might follow.

b. Nonlinear Finite-element Model. Finite-element model for the nonlinear analysis consists of the dam monolith and gap-friction elements. The foundation rock is not included in the model in order to reduce computational efforts. The tensile cracking at the base of the dam is modeled by introducing gap-friction elements between the dam and the rigid foundation. The gap-friction elements are nonlinear elements that can resist bearing and shear parallel to the bearing plane but not tension. The friction forces follow the Coulomb theory and thus are directly proportional to bearing forces in the element. Figure H-11 shows the dam finite-element model with 23 gap-friction elements between the dam and the rigid base. Except for the nonlinear gap-friction elements, the rest of the dam is assumed to remain elastic. Consequently, the dam monolith is represented by linear finite elements as described previously in Paragraph H-5a. The complete finite-element model consists of 1,493 linear shell elements with 23 nonlinear gap-friction elements.

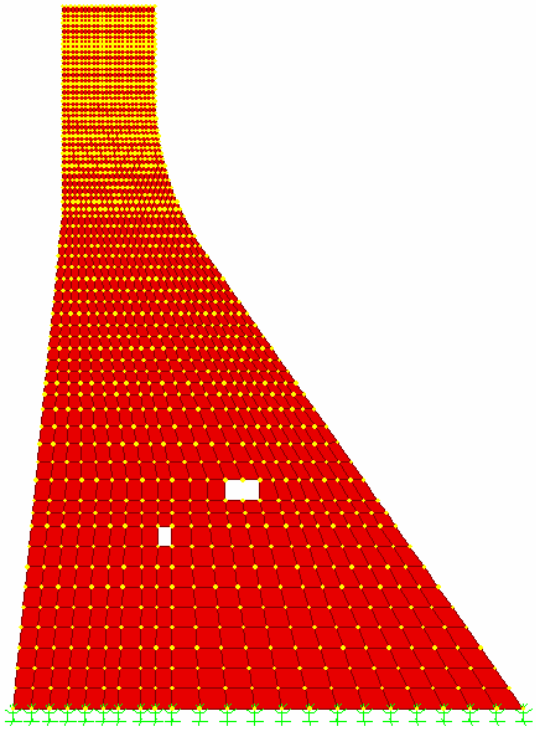

Figure H-11. Dam finite-element model with gap-friction elements

c. Selection of Parameters. The gap-friction elements used in this example have friction properties for shear deformation in the horizontal direction and gap behavior in the axial or vertical direction. The gap properties usually include zero tension resistance but the element can be preloaded so that the element could start with a certain amount of tension resistance. In this example, zero cohesion with a friction angle of 45 degrees were assumed for sliding along the dam-foundation contact surface. Tensile strength of the dam-foundation contact was assumed to be either 1.38 MPa (200 psi) or zero. Using these parameters the following two cases were evaluated:

(1) *Case-I*: No uplift pressure, $f_{interface}$ = 1.38 MPa (200 psi), = 45°

(2) *Case-II*: With uplift pressure, $f_{interface}$ = 0 MPa (0 psi), = 45°

d. Evaluation Loads. The nonlinear dynamic analysis was conducted for the combined action of static and earthquake loads. The static loads included gravity, hydrostatic pressures, and the uplift pressures, all of which were applied as initial loads. The uplift pressures, when applied, were assumed to vary linearly from the headwater to tailwater with no changes during the earthquake ground shaking. A zero tailwater was assumed. The earthquake loads included the same four acceleration time-history records discussed previously in Paragraph H-4.

H-7. Evaluation of Nonlinear Response

a. *Case-I*. The results for the case with 200 psi interface tensile strength and no uplift pressure are presented in Figures H-12 to H-16. Stress results in Figure H-12 show significant reduction in tensile stresses due to tensile cracking at the base of the dam. Not only tensile stresses at the base of the dam are now limited to 200 psi (i.e. interface tensile strength) but their magnitudes within the body of the dam have also dropped significantly. The maximum tensile stress of 200 psi occurs only at the heel of the dam, while the maximum tensile stresses near the upstream face of the dam are 40 to 80 psi. The stress results confirm the modeling assumption that only tensile cracking at the base of the dam needs to be modeled, because the cracked-base condition tends to relieve high tensile stresses elsewhere. Figure H-13 shows deflected shape at the time of maximum displacement. Thirteen gap-friction elements in the upstream side opened and slid during the earthquake ground shaking. This indicates that cracking starts at the heel of the dam and stops after propagating about half width of the base. Figure H-14 is a plot of gap opening for the gap-friction element at the heel of the dam. This figure indicates that the crack at the base of the dam repeatedly opens and closes during the earthquake excitation. Time histories of sliding displacements for 14 gap-friction elements that indicated opening and sliding are displayed in Figure H-15. This figure shows a permanent sliding displacement of about 0.04 inches at the heel of the dam, which reduces to zero toward the mid section of the base where the cracking stops. The downstream half of the base remains intact with no cracking or sliding. Note that the partial sliding of the upstream half of the base is caused by elastic deformation of the flexible dam monolith due to static and earthquake loads. Figure H-16 shows the horizontal displacement history at the top of the dam, where displacement due to hydrostatic pressure can be noted at the beginning and end of the record.

b. *Case-II*. The results for the case with uplift pressure and zero tension allowance at the base indicated similar reduction in tensile stresses, except that now tensile stresses at the base of the dam are zero and that the crack propagates through the entire base of the dam. Figure H-17 shows time histories of sliding displacements for all joints across the base of the dam. The sliding displacement varies from joint to joint due to deformations of the flexible dam. The sliding displacements are slightly higher for nodes closer to the heel and reduce as approaching the

toe. For a rigid dam, sliding displacements are the same for all nodes across the base. Figure H-18 displays horizontal displacement history for a crest nodal point, where the permanent displacement at the end of the record is evident. The results show an overall permanent displacement of about 0.8 inches. Although this permanent displacement is relatively small and does not appear alarming, the main concern is the post-earthquake stability condition of the dam under static loads. The post-earthquake static sliding factor of safety for the example dam was found to fall below unity. This is because the uplift forces have increased due to formation of crack at the base of the dam. Therefore the dam should be retrofitted and its shear resistance increased to remedy the situation.

H-8. Conclusions and Recommendations

Linear and nonlinear time-history analyses were used to assess earthquake performance of a typical non-overflow gravity dam section. The linear-elastic time-history analysis was employed to gain insight into the dynamic behavior of the dam, to account for transitory nature of earthquake ground shaking, and to identify potential modes of failure for the subsequent nonlinear time-history analysis. The results of linear-elastic time-history analyses were compared with the EM 1110-2-6051 performance acceptance criteria for gravity dams (see Paragraph 6.4d(1)). This comparison indicated that the example dam would suffer significant cracking along the base and should be assessed on the basis of nonlinear time-history analysis. The results also showed that instantaneous factors of safety obtained from the linear-elastic time-history analysis repeatedly fall below one, an indication that the dam would undergo sliding during the earthquake ground shaking. Subsequent nonlinear time-history analyses were carried out using gap-friction elements to model cracking and sliding along the dam-foundation contact. The nonlinear time-history results indicate that the dam will suffer cracking along its entire base and will undergo sliding with a permanent displacement offset of 0.8 inches in the downstream direction. Although this permanent offset may not be consequential, the post-earthquake static factor of safety for the cracked-base condition falls below one. The dam therefore becomes unstable after the earthquake shaking due to the pore pressure build up beneath the dam. The situation calls for remediation action. It is recommended conceptual remediation schemes be developed and implemented to increase shear resistance of the dam.

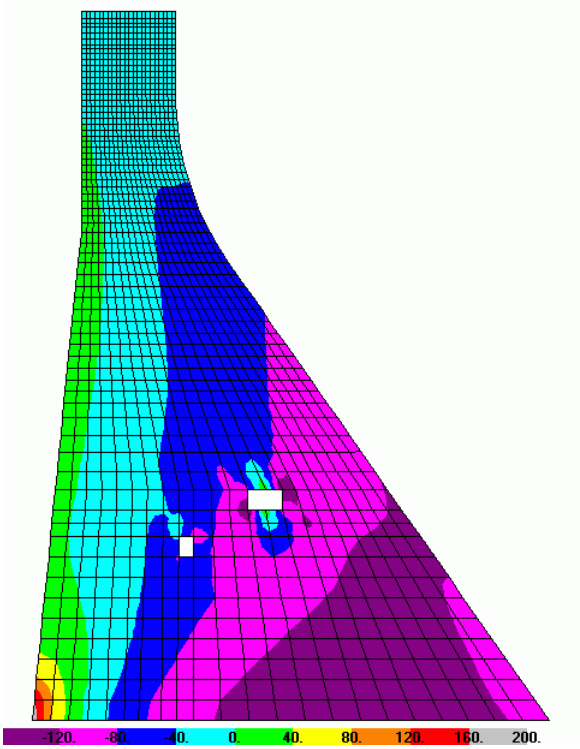

a) Loma Prieta - Nonlinear

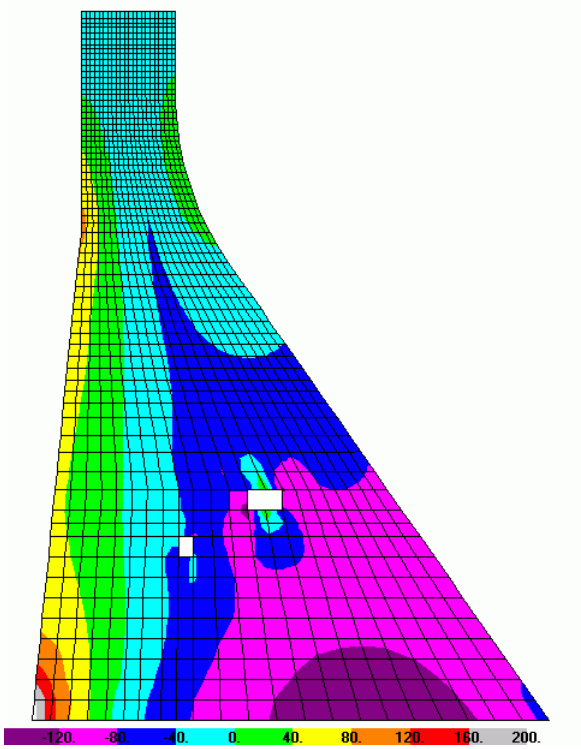

b) Northridge - Nonlinear

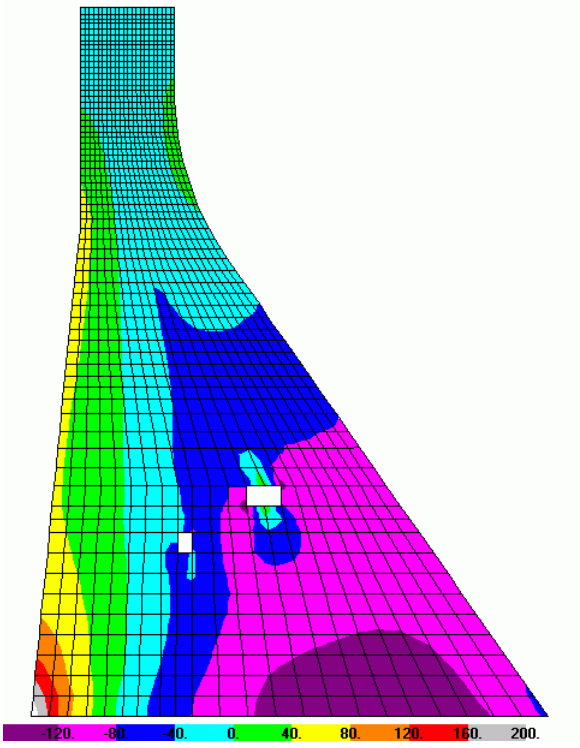

c) San Fernando - Nonlinear

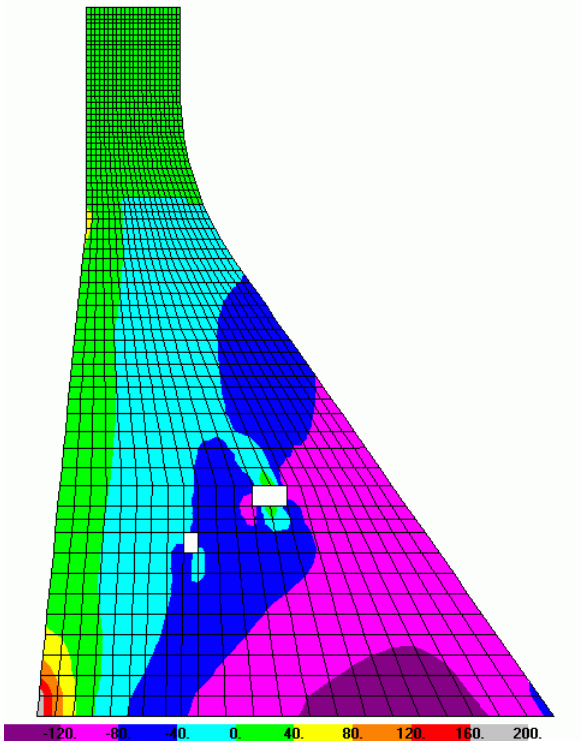

d) Pacoima – Nonlinear

Figure H-12. Envelopes of maximum vertical stresses from nonlinear TH analysis (psi)

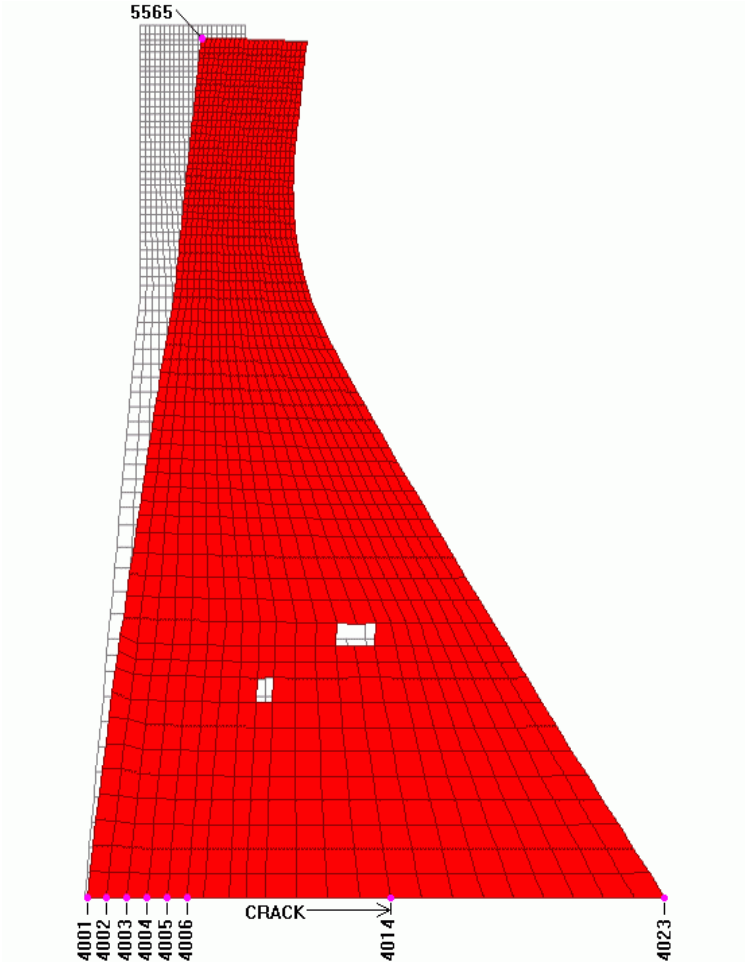

Figure H-13. Deflected shape at the time of maximum displacement. Also shown are 6 gap elements that experienced opening and sliding (San Fernando record)

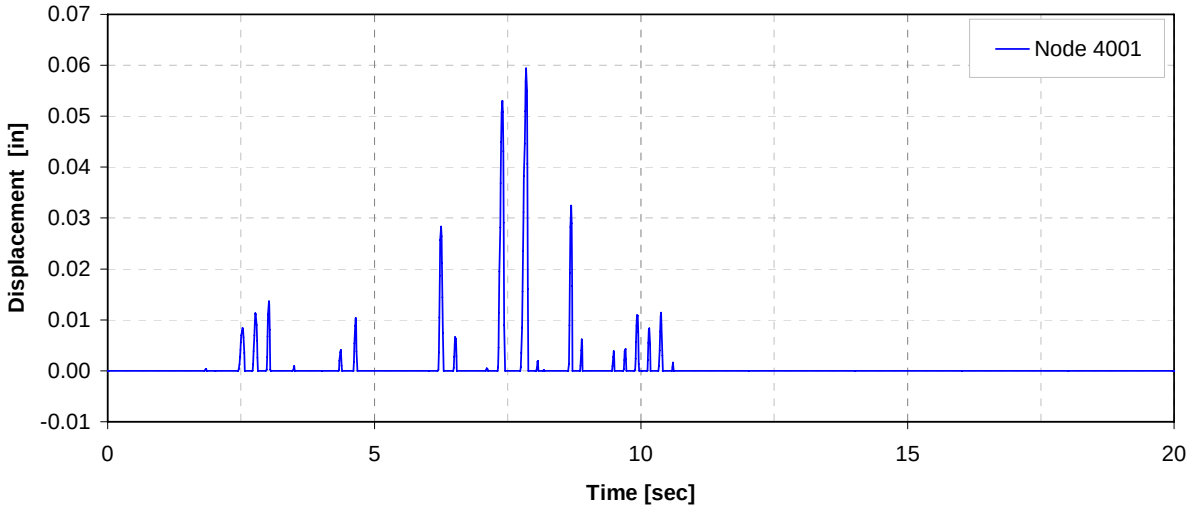

Figure H-14. Gap or crack opening at the heel of the dam (San Fernando record)

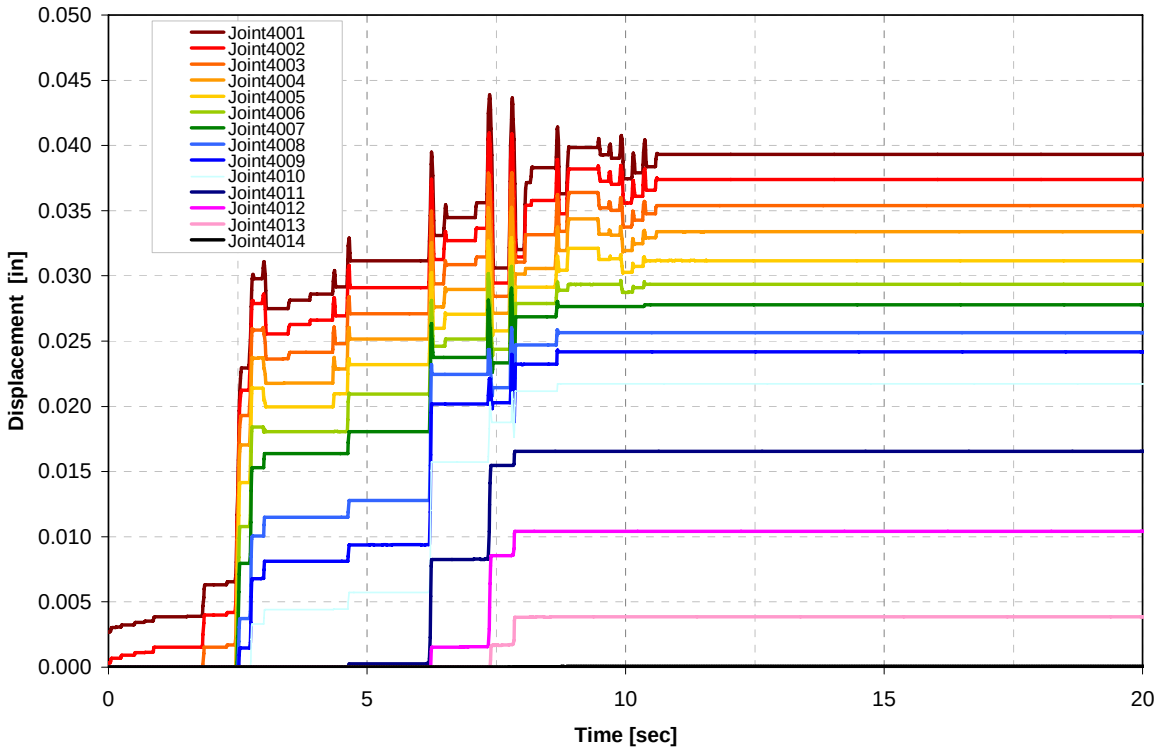

Figure H-15. Horizontal sliding displacements for gap elements located at Nodes 4001 to 4014 (San Fernando record)

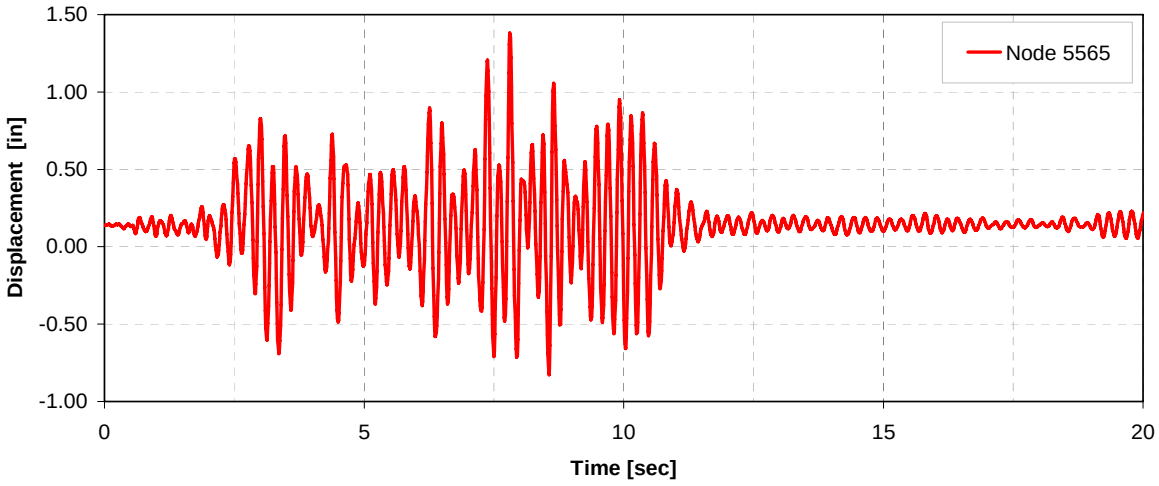

Figure H-16. Time history of horizontal displacement at the top of dam (San Fernando record)

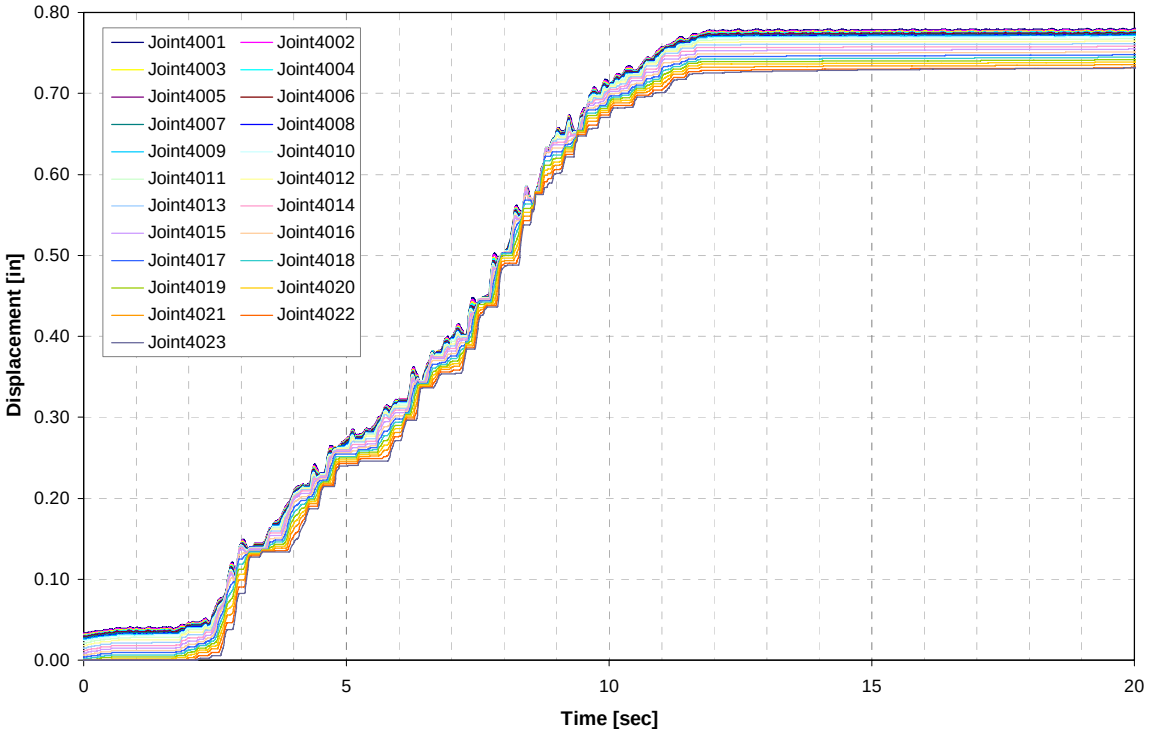

Figure H-17. Time histories of sliding displacements of nodal points at the base of the dam (San Fernando record)

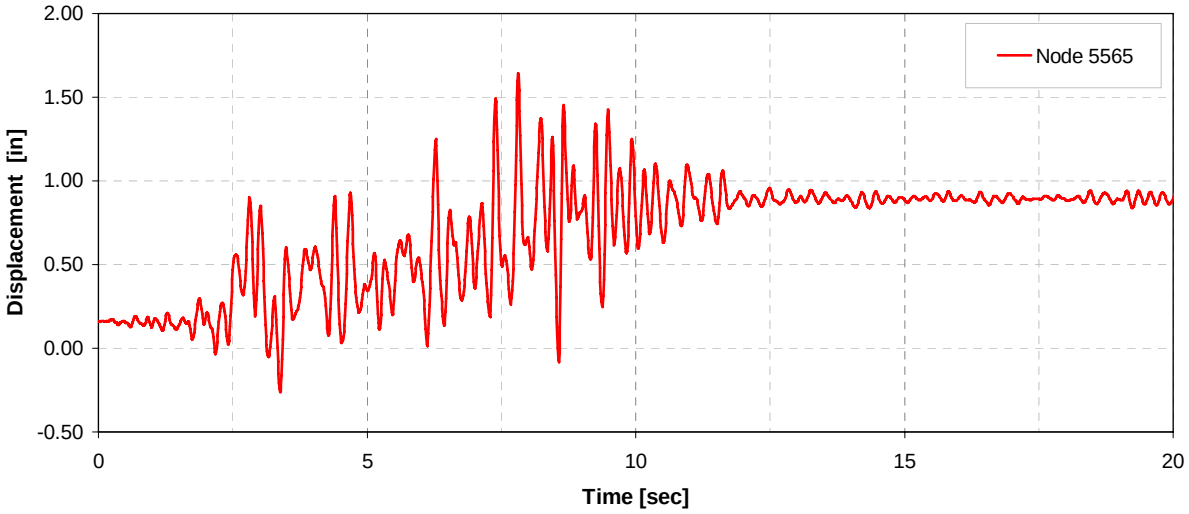

Figure H-18. Time history of horizontal displacement at the top of dam (San Fernando record)